JOURNAL OF SOLID STATE CHEMISTRY 117, 363–372 (1995)

The Ternary Yttrium Sulfides, CaY_2S_4, SrY_2S_4, and BaY_2S_4: Structures and Properties

C. K. Lowe-Ma and T. A. Vanderah[1]

Research Department, Naval Air Warfare Center, Weapons Division, China Lake, California 93555

and

Trudy E. Smith

Department of Chemistry, Connecticut College, New London, Connecticut 06320

Received April 22, 1994; in revised form September 19, 1994; accepted September 22, 1994

X-ray single-crystal structure determinations have confirmed that CaY_2S_4 crystallizes in the orthorhombic [Yb_3S_4]-type structure whereas SrY_2S_4 and BaY_2S_4 adopt the orthorhombic [$CaFe_2O_4$] structure. Both structure types feature three-dimensional frameworks built of edge- and corner-sharing [YS_6] octahedra. CaY_2S_4, in space group *Pnma*, has cell dimensions a = 12.953(3) Å, b = 3.8835(5) Å, c = 13.081(3) Å, Vol = 658.0(2) Å^3, Z = 4, and D_x = 3.494 g/cm^3 (M_F = 346.1). SrY_2S_4, in *Pmnb*, has a = 3.9775(6), b = 11.974(2), c = 14.294(2) Å, Vol = 680.8(2) Å^3, Z = 4, and D_x = 3.841 g/cm^3 for M_F = 393.7; BaY_2S_4, in *Pmnb*, has a = 4.0263(2), b = 12.2134(8), c = 14.484(1) Å, Vol = 712.23(9) Å^3, Z = 4, and D_x = 4.135 g/cm^3 for M_F = 443.4. Room temperature X-ray powder diffraction data for all three compounds and high-temperature unit cells for CaY_2S_4 are also reported. The overall average linear thermal expansion of CaY_2S_4 upon heating was found to be approximately 11.9 × 10^{-6}/°K as compared to that of 7.2 × 10^{-6}/°K found for ZnS. The onset oxidative decomposition temperatures for CaY_2S_4, SrY_2S_4, and BaY_2S_4 were observed to be 545, 565, and 590°C, respectively, as compared to 530°C for ZnS. The properties of these compounds indicate that they are potentially useful as infrared window materials.

INTRODUCTION

In the early 1960s Flahaut and co-workers investigated the structural chemistry of several series of yttrium- and rare-earth-containing binary and ternary sulfides using powder X-ray diffraction methods (1–4). CaY_2S_4 was reported to have a low-temperature orthorhombic structure analogous to that of Yb_3S_4 ($Yb^{2+}Yb_2^{3+}S_4$) and a high-temperature (T > 1100°C) orthorhombic form isostructural with [MnY_2S_4] (1, 2, 5). Tsai and Meschter (6) subsequently reported a powder pattern for orthorhombic "α-CaY_2S_4" (a = 12.89 Å, b = 13.03 Å, c = 3.87 Å) quenched from 1000°C that was consistent with the low-temperature form reported by Flahaut (see Ref. 7). However, in contrast to the earlier work, Tsai and Meschter (6) found high-temperature (T > 1120°C) "β-CaY_2S_4" to be monoclinic (a = 12.88 Å, b = 13.04 Å, c = 4.02 Å, β = 93.48° after quenching from 1200°C) (6). Other studies of Yb_3S_4($Yb^{2+}Yb_2^{3+}S_4$) and the related CaM_2S_4 series (M^{3+} = Y, Dy, Ho, Tm, Yb, Lu) have not provided consistent information about the high-temperature structure(s) of these compounds (8, 9). The variability in results may be related to sample differences; e.g., unless oxygen is rigorously excluded, oxysulfides may form.

X-ray powder diffraction studies of SrY_2S_4, BaY_2S_4, and PbY_2S_4 indicated that these compounds were isotypic with a structure distinctly different from that of "α-CaY_2S_4" (10). SrY_2S_4 and BaY_2S_4 were later found to be members of the $SrLn_2S_4$ and $BaLn_2S_4$ families (11) which form with the orthorhombic [$CaFe_2O_4$]-type structure analogous to the oxide congeners (12–15). Patrie *et al.* (11) prepared a single crystal of BaY_2S_4 for which cell parameters of a = 12.16 Å, b = 14.56 Å, and c = 4.06 Å were obtained by Weissenberg methods. The extinction conditions indicated space group *Pnma*; the empirical formula was used to rationalize two possible structures, both having all of the atoms residing on the mirror plane at $z = \frac{1}{4}$ ($y = \frac{1}{4}$ in the standard setting). Comparison of observed and calculated intensities for the X-ray powder diffraction pattern suggested the [$CaFe_2O_4$]-type structure. By analogy, the [$CaFe_2O_4$]-type structure was attributed to the structures of 10 $BaLn_2S_4$ compounds, 7 $SrLn_2S_4$ compounds, and SrY_2S_4. Unit cell parameters of a = 11.97 Å, b = 14.34 Å, and c = 3.99 Å were reported for SrY_2S_4 (11).

[1] Permanent address: Ceramics Division, NIST, Gaithersburg, MD 20899.

0022-4596/95 $12.00

Recent infrared studies of single crystals of CaY_2S_4 and SrY_2S_4 have indicated optical cut-offs of ~11.4 and 11.7 μm, respectively (16), suggesting that these compounds have significant potential as infrared window materials. The study reported here was undertaken to determine the full structural details of the compounds and to measure other properties pertinent to their use as optical ceramics.

EXPERIMENTAL

CaY_2S_4, SrY_2S_4, and BaY_2S_4 crystals were grown from eutectic halide fluxes with molar compositions $0.73CaCl_2$:0.27KCl (m.p. 640°C), $0.67SrCl_2$:0.33KCl (m.p. 620°C), and $0.44BaCl_2$:0.56KCl (m.p. 644°C), respectively. All syntheses were carried out in carbon crucibles enclosed in evacuated ($<10^{-4}$ Torr) silica ampoules that had been previously outgassed under vacuum at ≈900°C. Care was taken to minimize exposure of reaction mixtures to moisture, and fluxes were stored in a vacuum oven at 140°C. For CaY_2S_4 and SrY_2S_4, the charges for the crystal growth experiments were intimate 1 : 1 molar mixtures of the respective binary sulfides whereas for BaY_2S_4 the polycrystalline form of the compound was used (prepared by reacting a stoichiometric mixture of the binary sulfides at 1000°C for 1 month). Light tan CaY_2S_4 needles were obtained by heating a 1 : 10 (by weight) charge:flux mixture over 12 hr to 1050°C, soaking 18 days at 1050°C, step-cooling to 1000°C followed by cooling at 2°/hr to 900°C thereafter the temperature was cycled at 2°/hr up to 1025°C and down to 900°C three times, and finally cooled at 1°/hr to the flux solidification temperature after which the furnace was turned off. The cycling procedure yielded crystals of sufficiently good quality to be used for a structure determination, whereas without temperature cycling the crystals were of poor quality. Pale yellow SrY_2S_4 needles were grown by heating a 1 : 10 (by weight) charge:flux mixture over 20 hr to 1050°C, soaking 15 days at 1050°C, step-cooling to 1025°C followed by cooling at 5°/hr to 900°C; thereafter the temperature was cycled up to 1025°C (at 10°/hr) and down to 900°C (at 5°/hr) twice, and finally cooled at 10°/hr to the flux solidification temperature. Off-white BaY_2S_4 needles were obtained by heating a 1 : 9 (by weight) charge:flux mixture over 24 hr to 1125°C, soaking 16 days at 1125°C, step-cooling to 1100°C followed by cooling at 2.5°/hr to 925°C; thereafter the temperature was cycled up to 1100°C (at 15°/hr) and down to 925°C (at 2.5°/hr) twice, and finally cooled at 2.5°/hr to the flux solidification temperature. Crystals were separated from the flux by soaking in distilled water.

The chemical compositions of the crystals were confirmed by energy-dispersive X-ray spectroscopy (EDX) using a scanning electron microscope (Electroscan E-3, NORAN Voyager). Incorporation of K or Cl from the flux was not detected. Auger spectroscopic analyses of ternary sulfide crystals grown with the method described here have not detected bulk oxygen contamination. (17) Oxidative decomposition temperatures were determined by differential thermal analysis (DTA) using a DuPont 2100 thermal analyzer. Freshly ground crystals were analyzed under flowing oxygen at 1 atm; ZnS crystals grown by iodine vapor transport (16) served as a reference. The onset oxidative decomposition temperatures observed for CaY_2S_4, SrY_2S_4, and BaY_2S_4 were 545, 565, and 590°C, respectively, as compared to 530° for ZnS.

Powder patterns for crushed crystals of each of the three compounds were obtained on a Scintag PAD V ($2\theta/\theta$) diffractometer using nickel-filtered copper X-radiation; the diffractometer, radius 220 mm, is equipped with a liquid-nitrogen-cooled solid-state germanium detector and pulse-height discrimination. For all three powder patterns incident and diffracted beam Soller slits were in place; the divergence angle was 1.43°. For CaY_2S_4 the data were recorded with a step scan from 5°–100° (2θ) with 5 sec counting per 0.02° step (acceptance angle of 0.14°). For SrY_2S_4 and BaY_2S_4 the powder diffraction data were recorded with continuous scans at 1°/min; data were collected at intervals of 0.03° from 5°–80° (2θ) (SrY_2S_4) or 5°–90° (BaY_2S_4) (acceptance angle of 0.21°). After background correction, α_2-stripping, and computerized peak-picking, the resulting peak lists were edited by hand; the edited peak lists were used as input to the least-squares unit-cell parameter refinement program CELLSVD. (18) Refinement of a sample displacement error was included in the unit cell refinement. From the single-crystal structural data obtained in this study (below), simulated powder patterns were calculated for all three compounds using XPOW of SHELXTL-Plus/PC (Siemens). The calculated intensities are integrated intensities, which include Lorentz–polarization effects and multiplicity but not optical effects. Comparisons between the observed and calculated powder pattern intensities were evaluated using the intensity figure-of-merit, $I_x(N) = (1/N) \sum [|I_{calc} - I_{obs}|/I_{calc}]$. This figure-of-merit gives the average percent intensity difference for N (strong and moderately strong) lines with $I_{calc} > x\%$ relative intensity and was recently introduced to evaluate whether or not the most intense lines, those used primarily for identification, reliably represent the intensities from a sample of randomly oriented particles. (19).

High-temperature X-ray diffraction data were collected on a Scintag XDS-2000 θ/θ diffractometer equipped with an Edmund Buehler high-temperature furnace, a copper X-ray tube and a liquid-nitrogen-cooled germanium solid-state detector. Temperature measurements were made using a W/WRe thermocouple welded to the underside of the furnace's tantalum heating strip, which also served as the sample holder. No efforts were made to ascertain the exact sample temperature as ZnS was used as a com-

parison material. The furnace chamber was evacuated and a radiant surrounding heater was used to minimize temperature gradients. Data in intervals of 0.03° were recorded for CaY_2S_4 with continuous scans at 2.5°/min. After background correction, peak positions were obtained by deconvolution using split Pearson VII functions that included α_2. Refined unit cell parameters were obtained using CELLSVD (18); an error for sample displacement was included in each refinement.

The crystal morphology of CaY_2S_4 is typified by long, striated, fibrous crystals or flattened rods. A yellowish, flaw-free transparent flattened rod with natural face terminations was selected for data collection; the dimensions of the crystal were approximately 0.70 × 0.18 × 0.08 mm. The needle axis was found to be [010]; the faces of the rod were {100} and {001}. SrY_2S_4 crystallizes as brittle, elongated (often striated) reddish-colored rods. A very small chunky transparent rod with no visible striations was selected for data collection; dimensions were 0.060 × 0.060 × 0.160 mm with {011} as the major faces parallel to the rod axis and {001} as minor faces (in setting *Pmnb*). BaY_2S_4 is morphologically the same as SrY_2S_4 although pale yellow in color. Dimensions of the BaY_2S_4 crystal used for data collection were 0.13 × 0.15 × 0.36 mm.

Unit cell dimensions for the single crystals were obtained from a symmetry-constrained least-squares fit of 24 (CaY_2S_4), 25 (SrY_2S_4), or 40 (BaY_2S_4) computer-centered reflections on a Nicolet/Siemens R3 diffractometer with monochromated Mo$K\alpha$. Intensity data were collected on the R3 as $2\theta/\theta$ scans with monochromated Mo$K\alpha$. The ratio of background to scan time was 1.0 and scan ranges were $1° < K\alpha_1$ to $1° > K\alpha_2$. Check reflections during data collection were (040), (6, 2, −3), (0, 0, −10), measured every 109 reflections for CaY_2S_4; (−1, −1, 3) and (−1, 2, 6) (in *Pmnb*) measured every 114 reflections for SrY_2S_4; (111), (−2, −6, 0), and (0, −4, 6) (in *Pmnb*) measured every 109 reflections for BaY_2S_4. Additional experimental parameters are given in Table 1. Intensity data for all three crystals were corrected for Lorentz and polarization effects and for absorption. Empirical absorption corrections for CaY_2S_4 were based on azimuthal scans taken every 20° in ψ for 25 reflections distributed throughout the accessible portion of reciprocal space. The systematic absences in the data of all three crystals were indicative of space groups *Pnma* or $Pna2_1$ (in standard settings); the centrosymmetric space group (*Pnma* or *Pmnb*) was chosen for the structure solutions. Unit cell parameters were also obtained from a single crystal of SrY_2S_4, under a cold nitrogen gas stream, at room temperature, −80°, −120°, and −151° C using a symmetry-constrained least-square fits of 30 reflections computer-centered at each temperature on a Nicolet/Siemens R3 equipped with a Nicolet/Siemens LT2 cold (gas stream) nitrogen device.

Initial phasing for both CaY_2S_4 and SrY_2S_4 was accomplished by assigning yttrium to one "heavy" atom that exhibited reasonable octahedral coordination in the automatic Patterson interpretation. The structures were subsequently solved through a combination of Patterson interpretation and difference Fourier techniques. BaY_2S_4 was intitially phased by assigning Ba to the heaviest atom obtained from the automatic Patterson interpretation. All atoms in all three structures reside on the mirror plane, at special positions, point set 4*c*. All atoms in the three structures were refined anisotropically by minimizing $[\Sigma w(F_o - kF_c)^2]$ for $w = 1/[\sigma^2(F) + gF^2]$ with $g = 0.0010$ (CaY_2S_4), 0.0006 (SrY_2S_4), or $g = 0.0009$ (BaY_2S_4). In the refinement of SrY_2S_4, yttrium was assumed to have octahedral coordination and Sr was assumed to be in the eight-coordinate bicapped trigonal prismatic site. For each structure, a factor for isotropic extinction was included in the final cycles of refinement. During the final cycles of refinement of BaY_2S_4 two difference peaks symmetrically displaced from the Ba atom were observed. Much weaker difference peaks symmetrically displaced in the same orientation about each yttrium atom were also observed. The two extra peaks about Ba were modeled as partially occupied sites containing yttrium. The thermal parameters of the two extra sites were tied together and refined isotropically to $U_{iso} = 0.0045$; occupancies of the two sites refined to values of 0.0106(16) and 0.0094(14) or approximately 2(±0.3)% occupancy by yttrium. All calculations were performed using SHELXTL PLUS-PC (20). Final difference Fourier maps yielded peaks and troughs of +2.82 to −3.29 $e^-/Å^3$ for CaY_2S_4, +1.37 to −1.12 $e^-/Å^3$ for SrY_2S_4, and +5.05 to −5.22 $e^-/Å^3$ for BaY_2S_4.

RESULTS

Room temperature X-ray powder diffraction data for CaY_2S_4 and SrY_2S_4 are available in the supplementary material.[2] The powder diffraction pattern and unit cell parameters obtained for CaY_2S_4 (*Pnma*, $a = 12.9462(10)$ Å, $b = 3.8816(4)$ Å, and $c = 13.0692(8)$ Å for $\lambda = 1.540562$ Å) are in agreement with the limited data available in the literature (5, 7, 10). The strongest lines for SrY_2S_4 are consistent with the information available in reference (10); unit cell parameters reported here (*Pnma*, $a = 11.9652(13)$ Å, $b = 3.9754(4)$ Å, and $c = 14.2842(17)$ Å for $\lambda = 1.540562$

[2] See NAPS document No. 05209 for 24 pages of supplementary material. Order from ASIS/NAPS. Microfiche Publications, P. O. Box 3513, Grand Station, New York, NY 10163. Remit in advance $4.00 for microfiche copy or for photocopy $7.75 up to 20 pages plus $.30 for each additional page. All orders must be prepaid. Institutions and organizations may order by purchase order. However, there is a billing and handling charge for this service of $15. Foreign orders add $4.50 for postage and handling, for the first 20 pages, and $1.00 for additional 10 pages of materials, $1.50 for postage of any microfiche orders.

TABLE 1
Experimental Parameters and Refinement Results for CaY_2S_4 (Space Group *Pnma*), SrY_2S_4(Space Group *Pmnb*), and BaY_2S_4 (Space Group *Pmnb*)

	CaY_2S_4	SrY_2S_4	BaY_2S_4
Intensity data ($2\theta/\theta$ scan mode)			
Scan rate	2°–10°/min	4°–12°/min	2–10°/min (or 4–16°/min)
Octants	$h\ k\ -l$, $h\ k\ l$,	$h\ -k\ l$, $h\ k\ l$,	$-h\ -k\ -l$, $-h\ -k\ l$, (partial $h\ -k\ l$, $-h\ k\ l$, $h\ k\ l$)
2θ range	4° to 75°	4° to 60°	4° to 70°
Indices	$0 \le h \le 22$, $0 \le k \le 6$, $-22 \le l \le 22$	$-6 \le h \le 6$, $0 \le k \le 16$, $0 \le l \le 20$	$-7 \le h \le 1$, $-20 \le k \le 1$, $-24 \le l \le 24$
Number of reflections	3580	2337	4932
Absorption corrections	Empirical	Numerical	Numerical
Faces		{001}, {011}, {0, −1, 1}, {100}	{001}, {011}, {0, −1, 1}, {100}
Min/max Transmission	0.104/0.546	0.239/0.315	0.0534/0.1355
R_{merge}	0.032	0.023	0.049
Unique reflections	1847	1131	1764
With $\lvert F\rvert > 4\sigma$	1538	880	1542
Refinement			
R	0.045	0.032	0.044
wR	0.065	0.033	0.053
GoF	1.43	0.84	1.30

Å) agree with those previously reported in (11). To our knowledge, powder pattern data for BaY_2S_4 have not been reported and are given in Table 2; the unit cell parameters obtained in this study (Table 2) are in agreement with those obtained by Weissenberg methods from a single crystal (11).

The $I_x(N)$ intensity figure-of-merit is a new method being used to assess the validity of strong and moderately strong observed powder pattern intensities. The observed peak intensities for CaY_2S_4, SrY_2S_4, and BaY_2S_4, which were obtained from a *single mount* (and single scan) for each of the three compounds, were compared with the integrated intensities calculated for a sample of randomly oriented particles. This comparison facilitated an assessment of effects of the fibrous or needle-like morphology of the materials on the intensities of those lines most useful for identification. $I_x(N)$ will vary from 0 for no differences between observed intensities and calculated intensities to ∞ for (infinitely) large differences. Pragmatically, without including instrumental optical effects in the calculated intensities and for all but the most careful work involving averages of intensities obtained from multiple mountings of a sample, $I_x(N)$ is usually ~0.10–0.50 for the 10 to 20 most intense lines (19). $I_x(N)$ values greater than 0.50 are probably indicative of distorted peak intensities due to nonrandomness in the sample mount. In the case of CaY_2S4, although the calculated 100% line was also the observed 100% line, only 4 of the 7 most intense observed lines were included in the top 6 most intense calculated lines. The intensity figure-of-merit is $I_{20}(13) = 0.589$, i.e., for the 13 calculated lines with $I_{rel} \ge 20$ the average calculated and observed intensity difference is ~59%. The high figure-of-merit value reflects the fibrous nature of the CaY_2S_4 sample. For SrY_2S_4, although the observed and calculated 100% lines were not the same, $I_{20}(16) = 0.350$. In the case of BaY_2S_4, the observed and calculated 100% lines were the same but $I_{20}(14) = 0.477$.

The unit cell parameters of CaY_2S_4 as a function of uncorrected thermocouple temperature are given in Table 3 and shown graphically in Fig. 1. Curves were fit to the cell parameters as functions of the uncorrected temperature (Fig. 1) and from these curves the instantaneous changes in cell parameters were calculated (22). Thus, the linear thermal expansion for each cell axis, $(da/dT)/a = \alpha$, was obtained. For the a axis, the thermal expansion was found to vary from 17.4×10^{-6} (303 K) to 7.1×10^{-6} (524 K) to 19.6×10^{-6} (763 K). The shape of the curve for the b axis was similar and the thermal expansion was found to vary from 26.9×10^{-6} (303 K) to 7.5×10^{-6} (552 K) to 20.9×10^{-6} (763 K). The curve for the c axis was approximately linear, resulting in a thermal expansion

TABLE 2
X-ray Powder Diffraction Data for BaY_2S_4 at 18°C

h	k	l	$2\theta_{obs}$	I_{obs}	$2\theta_{CORR}$	$2\theta_{CALC}$	$2\Delta\theta^a$	d_{CORR}
1	0	2	14.176	4	14.218	14.222	−0.004	6.22417
2	0	2	18.970	14	19.012	19.013	−0.002	4.66419
3	0	1	22.649	2	22.690	22.691	0.000	3.91563
0	1	1	22.895	6	22.936	22.950	−0.014	3.87419
1	1	1	24.038	4	24.079	24.094	−0.015	3.69283
0	0	4	24.551	41	24.592	24.593	0.000	3.61695
3	0	2	25.063	100	25.104	25.097	0.008	3.54433
1	0	4	25.628	10	25.669	25.668	0.001	3.46759
1	1	2	26.342	13	26.383	26.380	0.003	3.37536
2	1	0	26.480	10	26.521	26.538	−0.017	3.35811
2	1	1	27.210	2	27.251	27.256	−0.005	3.26979
3	0	3	28.642	3	28.683	28.688	−0.005	3.10973
0	1	3	28.835	3	28.876	28.897	−0.021	3.08939
4	0	0	29.225	6	29.266	29.252	0.014	3.04910
1	1	3	29.793	28	29.834	29.828	0.005	2.99234
4	0	2	31.791	36	31.832	31.810	0.022	2.80894
3	0	4	33.091	4	33.131	33.117	0.015	2.70165
3	1	2	33.639	4	33.679	33.684	−0.005	2.65894
1	1	4	34.080	7	34.120	34.123	−0.003	2.62558
2	1	4	36.456	25	36.496	36.494	0.003	2.45993
4	1	0	36.925	14	36.965	36.966	−0.001	2.42979
4	1	1	37.464	11	37.504	37.502	0.002	2.39610
0	1	5	38.255	5	38.295	38.300	−0.005	2.34842
4	1	2	39.025	3	39.065	39.075	−0.010	2.30389
2	0	6	40.140	29	40.180	40.180	0.000	2.24249
2	1	5	41.110	3	41.150	41.158	−0.008	2.19185
3	0	6	43.564	12	43.603	43.600	0.003	2.07403
3	1	5	44.485	30	44.524	44.516	0.008	2.03325
6	0	1	44.911	12	44.950	44.975	−0.025	2.01496
5	1	2	45.120	7	45.159	45.204	−0.045[b]	2.00612
2	1	6	46.281	9	46.320	46.327	−0.008	1.95851
5	1	3	47.420	3	47.459	47.449	0.009	1.91414
4	0	6	48.021	7	48.060	48.058	0.002	1.89160
2	2	2	49.333	3	49.371	49.345	0.026	1.84437
1	1	7	50.119	4	50.157	50.153	0.005	1.81729
1	0	8	50.950	6	50.988	51.010	−0.022	1.78961
6	0	4	51.475	16	51.513	51.510	0.003	1.77260
2	1	7	51.929	6	51.967	51.915	0.052[b]	1.75818
3	2	2	52.211	9	52.249	52.291	−0.042[b]	1.74936
4	1	6	53.438	4	53.476	53.495	−0.019	1.71208
7	0	2	54.047	5	54.085	54.070	0.015	1.69423

Note. Refined unit cell parameters in *Pnma* are a = 12.2022(25) Å, b = 4.0185(6) Å, c = 14.4676(30) Å for a wavelength of 1.540562 Å. An error for sample displacement was included in the unit cell refinement. Multiply-indexed reflections were also included in the refinement. Smith-Snyder (21) F_N = 52(0.009, 91) for the 41 observed (indexed) reflections.

[a] $2(\theta_{CORR} - \theta_{CALC})$.

[b] $\Delta\theta$ exceeded the tolerance for inclusion in the design matrix during the final cycles of refinement.

TABLE 3
Unit Cell Parameters of CaY_2S_4 Obtained from High-Temperature X-Ray Powder Diffraction Data (λ = 1.540562 Å)

Apparent temperature (°C)	a (Å)	b (Å)	c (Å)
30	12.956(2)	3.8818(8)	13.077(1)
75	12.967(3)	3.8900(12)	13.088(2)
150	12.977(1)	3.8917(7)	13.0965(9)
225	12.986(1)	3.8947(6)	13.1074(7)
300	12.989(1)	3.8974(9)	13.123(1)
375	13.003(1)	3.9013(8)	13.1351(9)
500	13.024(2)	3.9073(12)	13.158(1)

that was approximately constant, varying from 11.4 × 10^{-6} (303 K) to 14.4 × 10^{-6} (763 K). The curves for instantaneous thermal expansion were fit to quadratic functions of temperature, resulting in the equations

$$\alpha = 6.5197 \times 10^{-5} - 2.2253 \times 10^{-7} \cdot T + 2.1321 \times 10^{-10} \cdot T^2 \text{ for } a,$$
$$\alpha = 10.165 \times 10^{-5} - 3.3964 \times 10^{-7} \cdot T + 3.0641 \times 10^{-10} \cdot T^2 \text{ for } b,$$
$$\alpha = 9.3710 \times 10^{-6} + 6.7043 \times 10^{-9} \cdot T - 1.3191 \times 10^{-13} \cdot T^2 \text{ for } c,$$

Note, however, that these equations should be considered approximate as they were obtained from curve-fitting sensitive to distortion from temperature errors. High-temperature X-ray diffraction data for ZnS (crushed crystals of sphalerite) were obtained under similar conditions. The unit cell volumes obtained for ZnS and CaY_2S_4 are compared in Fig. 2. Applying the first-order approximation $\alpha_v = \alpha(a) + \alpha(b) + \alpha(c) = 3\bar{\alpha}$ to the volume data in Fig. 2 yields an overall average linear thermal expansion, $\bar{\alpha}$ = 11.9 × 10^{-6}/°K for CaY_2S_4. A value of $\bar{\alpha}$ = 7.2 × 10^{-6}/°K was obtained for ZnS and compares favorably with values of 6.9 × 10^{-6} for IRTRAN2 (23a) and 7.85 × 10^{-6} for Raytran Multispectral Grade ZnS (23b). The average thermal expansion for CaY_2S_4 is similar to

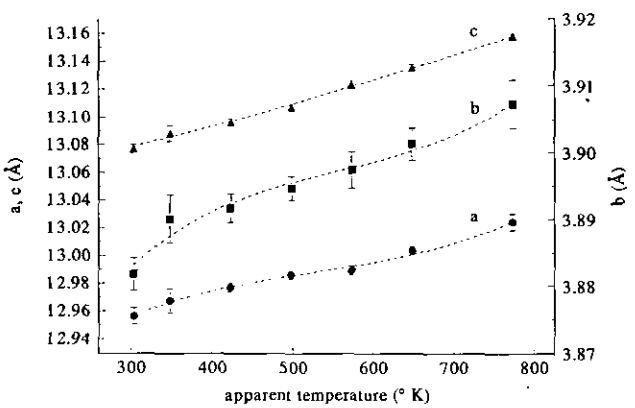

FIG. 1. Refined unit cell parameters of CaY_2S_4 calculated from high-temperature X-ray powder diffraction data are shown plotted against the nominal thermocouple temperature of the heating strip/sample holder. Error bars are three times the estimated standard deviation. The instantaneous thermal expansions along the cell edges, $(da/dT)/a$, were calculated from the fitted curves shown by the dashed lines.

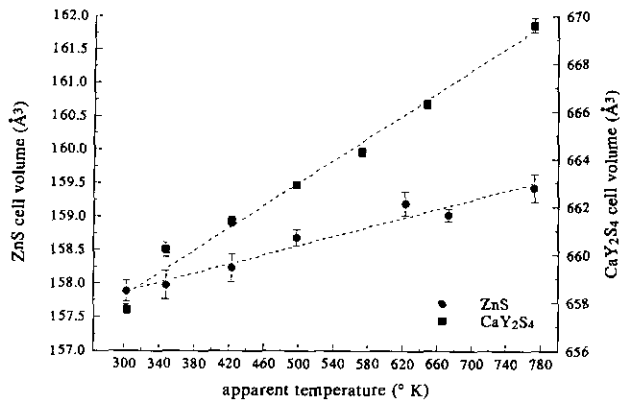

FIG. 2. Variation of unit cell volumes for ZnS and CaY_2S_4 are shown plotted against the nominal thermocouple temperature. Error bars are three times the estimated standard deviation.

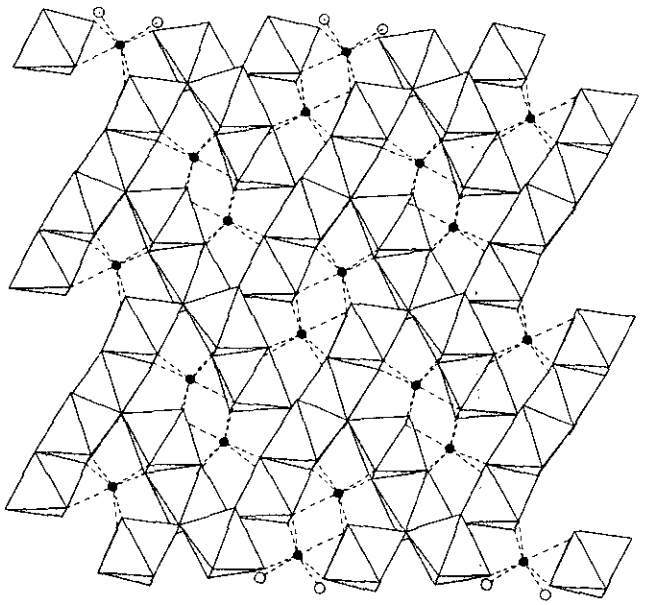

FIG. 3. This figure illustrates the connectivity of $[YS_6]$ octahedra in CaY_2S_4, a $[Yb_3S_4]$-type structure. Black spheres represent the seven-coordinate Ca atoms. The open spheres represent S atoms which are fragments of $[YS_6]$ octahedra not shown.

the $\bar{\alpha} = 9.7\text{–}13.7 \times 10^{-6}$/°K reported for (tetragonal) MgF_2 (24), also an infrared optical window material.[2]

The changes in unit cell parameters at low-temperatures for SrY_2S_4 were found to be linear resulting in coefficients of thermal expansion of $\alpha = 20.1 \times 10^{-6}$ along a, $\alpha = 6.37 \times 10^{-6}$ along b (short axis), $\alpha = 5.48 \times 10^{-6}$ along c (in setting *Pnma*) over the temperature range −150° to +18°C.

Final atomic coordinates and anisotropic thermal parameters obtained from the single-crystal structure determinations are given in Tables 4, 5, and 6. Observed and calculated structure factors along with complete tables of bond lengths and angles are available as supplementary material.[2]

DISCUSSION

CaY_2S_4 has been found to be isostructural with $CaYb_2S_4$ (25), $CaLu_2S_4$ (26), and Yb_3S_4 (27), in accord with the previous reports (1–3). The structure is related to that of warwickite ($(Mg, Fe, Ti)_2BO_4$) (28) and is formed of strings of four edge-sharing YS_6 octahedra as illustrated in Fig. 3. Each string of four octahedra is a cross-section of an infinite ribbon ($4 \times 1 \times \infty$) extending along b. The octahedra share edges along the ribbons and, thus, form four-octahedra-wide strips of the $CdCl_2$ structure. The ribbons are interconnected by vertex sharing to form an overall three-dimensional framework containing channels of capped trigonal prismatic sites that accommodate the calcium atoms. Two crystallographically distinct yttrium sites occur; the near-octahedral geometry about each is partially constrained by symmetry, resulting in four unique bond lengths in each octahedron. The Y–S bond lengths about Y(1) range from 2.706(1) to 2.799(2) Å; those about Y(2) range from 2.715(1) to 2.749(2), with a mean value of 2.737(26) Å for both octahedra. This value is in good agreement with the sum of the ionic radii (29) for

TABLE 4
Atomic Coordinates and Anisotropic Thermal Parameters for CaY_2S_2 (in *Pnma*)

	x	y	z	U_{11}	U_{22}	U_{33}	U_{13}
Ca	0.36912(7)	0.2500	0.41743(8)	0.0040(3)	0.0076(4)	0.0198(4)	0.0017(3)
Y(1)	0.39197(4)	0.7500	0.08311(4)	0.0056(2)	0.0094(2)	0.0222(3)	0.0011(2)
Y(2)	0.35446(4)	0.7500	0.70405(4)	0.0050(2)	0.0092(2)	0.0191(2)	−0.0002(2)
S(1)	0.21771(10)	0.2500	0.76401(11)	0.0067(4)	0.0112(5)	0.0196(5)	0.0010(4)
S(2)	0.03318(10)	0.2500	0.38235(10)	0.0069(4)	0.0121(5)	0.0182(5)	0.0026(4)
S(3)	0.24491(10)	0.7500	0.52559(11)	0.0051(4)	0.0096(5)	0.0185(5)	−0.0007(4)
S(4)	0.47203(10)	0.2500	0.61759(11)	0.0050(4)	0.0101(5)	0.0232(5)	0.0022(4)

Note. The anisotropic displacement exponent takes the form $-2\pi^2(h^2a^{*2}U_{11} + \cdots + 2kLb^*c^*U_{23})$.

TABLE 5
Atomic Coordinates and Anisotropic Thermal Parameters for SrY_2S_2 (in *Pmnb*)

	x	y	z	U_{11}	U_{22}	U_{33}	U_{23}
Sr	0.7500	−0.24241(6)	0.66171(5)	0.0089(3)	0.0120(3)	0.0100(3)	−0.0006(2)
Y(1)	0.2500	0.06781(6)	0.11024(5)	0.0074(3)	0.0087(3)	0.0075(3)	−0.0008(2)
Y(2)	0.7500	−0.08092(5)	0.39911(5)	0.0071(3)	0.0082(3)	0.0082(3)	−0.0004(2)
S(1)	0.2500	−0.02191(16)	0.28411(13)	0.0083(3)	0.0149(8)	0.0091(8)	0.0038(6)
S(2)	0.7500	−0.08631(14)	0.07845(12)	0.0084(8)	0.0079(7)	0.0088(7)	0.0009(6)
S(3)	0.7500	0.20743(14)	0.17432(12)	0.0086(8)	0.0086(7)	0.0118(8)	−0.0002(6)
S(4)	0.2500	−0.13026(15)	0.52649(12)	0.0094(8)	0.0087(7)	0.0085(7)	0.0022(6)

Note. The anisotropic displacement exponent takes the form $-2\pi^2(h^2a^{*2}U_{11} + \cdots + 2kLb^*c^*U_{23})$.

S^{2-} and Y^{3+} (2.74 Å). As compared to the ideal value of 90°, the S–Y–S bond angles in the octahedra range from 84.4° to 101.8°. The calcium atom in the capped trigonal prismatic site is coordinated by five sulfur atoms at distances ranging from 2.866(1) to 2.938(2) Å plus two at a slightly longer distance of 3.010(2) Å; the overall mean Ca–S distance is 2.925(63) Å. This value is consistent with those reported for isostructural $CaLu_2S_4$ (26) (mean Ca–S distance of 2.910(54) Å) and $CaYb_2S_4$ (25) (mean Ca–S distance of 2.914(52) Å) and with the sum of the ionic radii (2.90 Å). (29). The coordination differs about the four crystallographically distinct sulfurs with S(1) and S(3) coordinated by five cations (three Y and two Ca), S(4) is also five-coordinate but to two Y and three Ca, and S(2) is coordinated by four yttrium atoms.

In accord with the findings of Patrie *et al.* (11), SrY_2S_4 and BaY_2S_4 have been found to be isostructural with $CaFe_2O_4$. The structure consists of edge-shared double rutile chains of $[YS_6]$ octahedra connected at the vertices to form channels of bicapped trigonal prismatic sites containing the larger Sr or Ba cations (Fig. 4). The octahedral Y–S distances range from 2.675(1) to 2.760(1) Å in SrY_2S_4 and from 2.695(2) to 2.765(1) Å in BaY_2S_4; the overall mean distances are 2.732(32) and 2.744(25) Å, respectively. These distances are in good agreement with the sums of the ionic radii (29). The mean Sr–S distance about the trigonal prismatic site is 3.093(10) Å with the two capping S atoms at an average distance of 3.29 Å; the mean Ba–S distance is 3.208(38) Å with the two capping atoms at an average distance of 3.35 Å. The sums of the ionic radii are 3.10 and 3.26 Å, respectively (29). The observed Ba–S distances compare favorably with the mean trigonal prismatic (3.217(13) Å) and average capping distance (3.38 Å) reported for isostructural $BaSm_2S_4$ (30). Although four crystallographically unique sulfurs exist in the SrY_2S_4 and BaY_2S_4 structures, only two different types of environments are found. In both environments each sulfur is bonded to two barium atoms and three yttrium atoms. S(1) has approximately trigonal bipyramidal coordination with two (somewhat distant) barium atoms as the axial atoms and the three yttrium atoms as the equatorial atoms. S(2), S(3), and S(4) all have approximately square pyramidal coordination; two barium (or strontium) atoms and two yttrium atoms lie in a plane to form the base while the third yttrium is above forming the pyramid. The sulfur is out of the plane of the base by 0.30 to 1.00 Å.

Shown in Fig. 5 is a structure-field map for AB_2S_4 compounds in which structure types are delineated by cationic size. In this figure, only $A^{2+}B_2^{3+}S_4$ compounds containing similar elements, A^{2+} = Mg, Ca, Sr, Ba, Zn, Pb, Eu, Sm, Yb, and B^{3+} = Sc, Y, La, *Ln* (Ce to Lu), have been included (11, 25–27, 30–42). Clear separation

TABLE 6
Atomic Coordinates and Anisotropic Thermal Parameters for BaY_2S_2 (in *Pmnb*)

	x	y	z	U_{11}	U_{22}	U_{33}	U_{23}
Ba	0.2500	0.24235(3)	0.16168(3)	0.0083(2)	0.0072(2)	0.0107(2)	0.0004(1)
Y(1)	0.2500	0.06727(5)	0.39151(4)	0.0075(2)	0.0062(2)	0.0086(2)	0.0008(2)
Y(2)	0.2500	0.7911(5)	−0.10154(4)	0.0070(2)	0.0057(2)	0.0092(2)	0.0001(2)
S(1)	0.7500	0.02173(12)	−0.21696(10)	0.0094(5)	0.0094(6)	0.0087(6)	−0.0017(4)
S(2)	0.2500	0.08198(12)	0.57716(10)	0.0073(5)	0.0053(5)	0.0100(6)	−0.0004(4)
S(3)	0.7500	0.12510(12)	0.02345(10)	0.0080(5)	0.0059(6)	0.0101(6)	−0.0009(4)
S(4)	0.7500	0.20738(12)	0.33595(11)	0.0083(6)	0.0044(5)	0.0144(6)	0.0010(5)

Note. The anisotropic displacement exponent takes the form $-2\pi^2(h^2a^{*2}U_{11} + \cdots + 2kLb^*c^*U_{23})$.

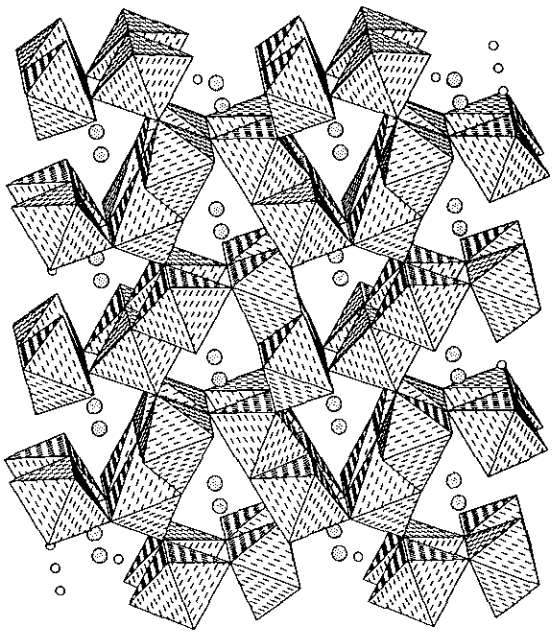

FIG. 4. This figure illustrates the connectivity of $[YS_6]$ octahedra in SrY_2S_4 and, analogously, BaY_2S_4; both have a $[CaFe_2O_4]$-type structure. The larger dotted spheres represent eight-coordinate Sr or Ba atoms. The smaller open spheres represent S atoms which are fragments of $[YS_6]$ octahedra not shown.

of structure types is observed in agreement with earlier maps (35, 43). These structure-field maps confirm Flahaut's early comments that cationic size is important in determining the type of structures adopted (2, 44–47), even though the bonding in sulfides would be expected to be more covalent than in oxides. Other structure-field maps using "bond-stretching force constants" and radius ratios (48) or using pseudopotential radii (49) have been constructed, but do not provide any additional insight beyond what can be gleaned from Fig. 5.

Although cationic size has been effective in delineating structure types, other electronic effects could play a role. Bond–valence sums, calculated from nearest-neighbor (bonding) distances, can reflect the underlying electronic interatomic interactions (50–52). However, when the bond-valence sums about A^{2+} and B^{3+} (52) are plotted against each other, little differentiation of structure types is found. Some differentiation of structure types is found for bond–valence sums plotted as a function of the ionic radius of B^{3+}, but the most distinct differentiation between structure types occurs when the bond–valence sums about A^{2+} and/or B^{3+} are plotted against the ionic radius of A^{2+}, Fig. 6. This suggests that the size of A^{2+} *is* important in determining the structure type of $A^{2+}B_2^{3+}S_4$ compounds with elements A^{2+} = Zn, Cd, Ca, Sr, Pb, or Ba and B^{3+} = Sc, Lu, Yb, Tm, Er, Y, or Sm. In addition, Fig. 6 suggests that the structural stability region for the Yb_3S_4 structure is much more chemically limited than that of the [spinel]- and $[CaFe_2O_4]$-type structures.

Structure-field maps, such as those described above, depend on having a set of consistent ionic radii. Although yttrium is not, strictly speaking, a rare-earth element, much of its chemistry is similar to the rare earths; its properties in sulfides are such that Flahaut (44) placed its apparent size between that of dysprosium and erbium. However, if the unit cell volumes of the series of compounds $A^{2+}Ln_2S_4$, A^{2+} = alkaline earth (Mg, Ca, Sr, Ba), are plotted against the trivalent ionic radii for six-coordi-

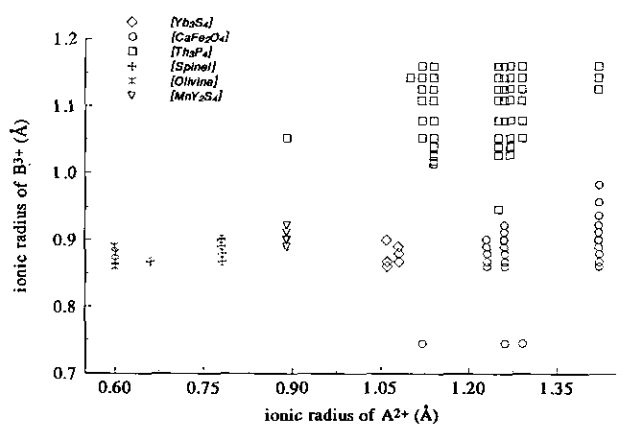

FIG. 5. A structure-field map delineated by cationic radii (29) is plotted for $A^2 + B_2^{3+}S_4$ compounds with A^{2+} = Mg, Ca, Sr, Ba, Zn, Pb, Eu, Sm, Yb, and B^{3+} = Sc, Y, La, *Ln* (Ce to Lu). A clear separation of structure types is observed.

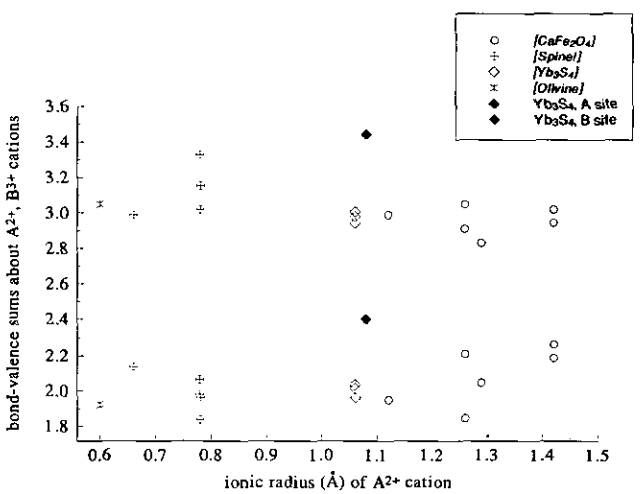

FIG. 6. Bond–valence sums about the cations are plotted as a function of the ionic radius of A^{2+} for $A^{2+}B_2^{3+}S_4$ compounds $ZnLu_2S_4$ (42), $CdYb_2S_4$ (41), $CdTm_2S_4$ (41), $CdEr_2S_4$ (54), CdY_2S_4 (40), $CaLu_2S_4$ (26), $CaYb_2S_4$ (25), CaY_2S_4 (this work), $CaSc_2S_4$ (32), $SrSc_2S_4$ (32), SrY_2S_4 (this work), $PbSc_2S_4$ (32), BaY_2S_4 (this work), $BaSm_2S_4$ (30), and Yb_3S_4 (27). The resulting separation of structure types suggests that the size of the divalent cation is important in determining structure type.

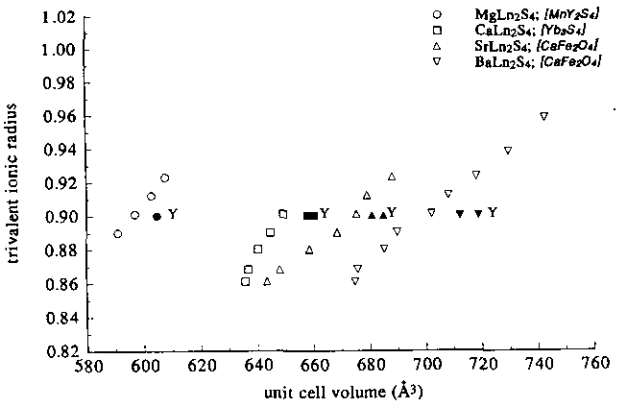

FIG. 7. The variation of unit cell volume with trivalent B^{3+} radius (29) is plotted for $A^{2+}B_2^{3+}S_4$, A^{2+} = Mg, Ca, Sr, or Ba, and B^{3+} = Y or rare earth. Unit cell data were taken from (11, 25, 34, 43) and this work. Data points for the yttrium-containing compounds are filled. Note that all of the yttrium-containing compounds are off the curves, suggesting that the effective ionic radius for yttrium in these sulfides is somewhat larger than expected.

nate *Ln* (29), as shown in Fig. 7, an anomaly becomes apparent. The trivalent ionic radius for octahedral yttrium in these sulfides appears to be noticeably larger than the value given by Shannon (29). Yet, in a similar plot of $SrLn_2O_4$ and $BaLn_2O_4$ compounds (Fig. 8), yttrium falls at the expected position on the curves. In the more polarizable sulfide series, the absence of inner-shell *f* electrons in yttrium may lead to increased ionicity and longer bond distances relative to the other rare earths. Thus, the increase in apparent yttrium size in the ternary sulfides (Fig. 7) could indicate decreased covalence and effects related to the principle of "maximal volume" (53).

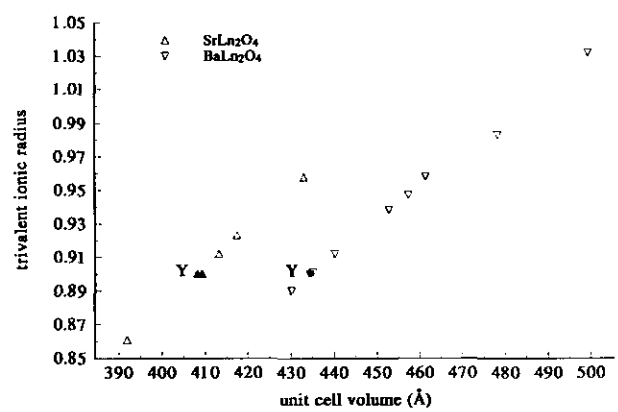

FIG. 8. The variation of unit cell volume with trivalent Ln^{3+} radius (29) for $SrLn_2O_4$ and $BaLn_2O_4$ compounds crystallizing in space group *Pnma* is shown. Unit cell data were taken from (12, 13, 15, 55). Data points for the yttrium-containing compounds are filled. Note that in contrast to the positions of the ternary yttrium sulfides in Fig. 7, the ternary yttrium oxide compounds fall at the expected positions.

CONCLUSIONS

Single-crystal structure determinations on CaY_2S_4, SrY_2S_4, and BaY_2S_4 have confirmed that CaY_2S_4 crystallizes with the $[Yb_3S_4]$-type structure whereas the Sr and Ba compounds crystallize with the $[CaFe_2O_4]$-type structure. Structure-field maps and plots of bond–valence sums versus divalent cation size suggest that for chemically similar divalent cations the structure type formed *is* to a large extent dependent on the size of the divalent cation. Yttrium in these particular ternary sulfides appears to exhibit a larger ionic radius than that observed in analogous oxides. CaY_2S_4, SrY_2S_4, and BaY_2S_4 were found to exhibit better oxidative stability than ZnS. The high-temperature linear thermal expansion coefficients of CaY_2S_4 and the low-temperature coefficients of SrY_2S_4 are significantly anisotropic; the overall average linear thermal expansion of CaY_2S_4 is greater than that of ZnS but similar to that of MgF_2. The oxidative stability of these octahedrally based three-dimensional ternary sulfides coupled with their long-wavelength infrared transparency (16) suggest that these compounds maybe useful as infrared window materials.

ACKNOWLEDGMENTS

The authors are grateful to M. W. Decker for assistance in sample preparation, to R. C. Scheri for the SEM/EDX analyses, and to S. B. Robie and A. Christensen (Scintag) for collection of the high-temperature X-ray powder diffraction data. This work was supported by the Office of Naval Research and NAWCWPNS internal research funds.

REFERENCES

1. J. Flahaut, *in* "(Fifth) Rare Earth Research Conference," Iowa State University, Ames, Iowa, Sept. 1965 (DTIC #AD 627223).
2. J. Flahaut, *in* "Progress in the Science and Technology of the Rare Earths," (L. Eyring, Ed.), Vol. 3, p. 209. Pergamon Press, New York, 1968, and references therein.
3. J. Flahaut, *in* "Handbook on the Physics and Chemistry of Rare Earths," (K. A. Gschneidner, Jr. and L. Eyring, Chap. 31, p. 1. North-Holland, Amsterdam, 1979, and references therein.
4. A. A. Eliseev and G. M. Kuzmichyeva, *in* "Handbook on the Physics and Chemistry of Rare Earths," (K. A. Gschneidner Jr. and L. Eyring, Eds.), Vol. 13, p. 191, Elsevier Science Publishers, New York, 1990.
5. (a) J. Flahaut, L. Domange, and M. Patrie, *Bull. Soc. Chim. Fr.* 105 (1961); (b) J. Flahaut, L. Domange, and M. Patrie, *C. R. Acad. Sci. Paris* **251,** 2535 (1960).
6. H. L. Tsai and P. J. Meschter, *J. Electrochem. Soc.* **128**(10), 2229 (1981).
7. Powder Diffraction File, PDF #17-244. JCPDS International Centre for Diffraction Data, Newtown Square, Pennsylvania, 1992.
8. C. O. Diaz and B. G. Hyde, *Acta Crystallogr. Sect. B* **39,** 569 (1983).
9. M. Patrie and J. Flahaut, *C. R. Acad. Sci. Paris* **264,** 395 (1967).
10. J. Flahaut, L. Domange, and M. Patrie, *Bull. Soc. Chem. Fr.*, 159 (1962).
11. M. Patrie, A. M. Golabi, J. Flahaut, and L. Domange, *C. R. Acad. Sci. Paris* **259,** 4039 (1964).

12. Hk. Müller-Buschbaum, *Z. Anorg. Allg. Chem.* **358,** 138 (1963).
13. E. Paletta and Hk. Müller-Buschbaum, *J. Inorg. Nucl. Chem.* **30,** 1425 (1968).
14. R. L. Barry and R. Roy, *J. Inorg. Nucl. Chem.* **29,** 1243 (1967).
15. G. A. Costa, M. Ferretti, M. L. Fornasini, E. A. Franceschi, and G. L. Olcese, *Powder Diffr.* **4**(1), 24 (1989).
16. M. P. Nadler, C. K. Lowe-Ma, T. A. Vanderah, *Mater. Res. Bull.* **28**(12), 1345 (1993).
17. D. O. Kipp, C. K. Lowe-Ma, and T. A. Vanderah, *Chem. Mater.* **2**(5), 506 (1990).
18. C. K. Lowe-Ma, "Refinement of Unit Cell Parameters by Least-Squares: Comments on an Old Technique and the Development of a New Computer Program," NAWCWPNS Technical Publication 8128 (UNCLASSIFIED), China Lake, CA, September 1993.
19. C. K. Lowe-Ma, *Powder Diff.* **6**(1), 31 (1991).
20. G. Sheldrick, "SHELXTL PLUS-PC Version 4.1/360," Siemens Analytical X-ray Instruments, Inc., 1990.
21. G. S. Smith and R. L. Snyder, *J. Appl. Crystallogr.* **12,** 60 (1979).
22. R. S. Krishnan, R. Srinivasan, S. Devanarayanan, "Thermal Expansion of Crystals," p. 13. Pergamon Press, New York, 1979.
23. (a) Y. S. Touloukian, R. K. Kirby, R. E. Taylor, and T. Y. R. Lee, *in* "Thermal Expansion of Nonmetallic Solids," Thermophysical Properties of Matter, Vol. 13, p. 1232. IFI/Plenum, New York, 1977; (b) C. A. Klein, "Compendium of Property Data for Raytran Zinc Selenide and Raytran Zinc Sulfide," Raytheon Publication RAY/RD/T-1154, 31 August 1987. See also C. Willingham, C. Klein, and J. Pappis *in* "Laser-Induced Damage in Optical Materials: 1981," NBS Special Publication 638, p. 53. Washington, DC, 1983.
24. D. M. Bailey, F. W. Calderwood, J. D. Greiner, O. Hunter, Jr., J. F. Smith, and R. J. Schiltz, Jr., *J. Am. Ceram. Soc.* **58**(11, 12), 489 (1975).
25. J. D. Carpenter and S.-J. Hwu, *J. Solid State Chem.* **97,** 332 (1992).
26. N. Rodier and V. Tien, *C. R. Acad. Sci. Paris* **284,** 909 (1977).
27. R. Chevalier, P. Laruelle, and J. Flahaut, *Bull. Soc. Fr. Mineral. Cristallogr.*, 564 (1967).
28. B. G. Hyde and S. Andersson, "Inorganic Crystal Structures," p. 164. Wiley, New York, 1989.
29. R. D. Shannon, *Acta Crystallogr. Sect. A* **32,** 751 (1976).
30. J. D. Carpenter and S.-J. Hwu, *Acta Crystallogr. Sect. C* **48,** 1164 (1992).
31. S. A. Ring and M. Tecotzky, *Inorg. Chem.* **3**(11), 1654 (1964).
32. D. J. W. IJdo, *Acta Crystallogr. Sect. B* **38,** 1549 (1982).
33. M. Patrie, M. Guittard, and M-P. Pardo, *Bull. Soc. Chim. France,* 3832 (1969).
34. M. Patrie and R. Chevalier, *C. R. Acad. Sci. Paris C* **263,** 1061 (1966).
35. P. L. Provenzano and W. B. White, "Synthesis and Crystal Chemistry of Sulfides and Tellurides with the Th_3P_4 Structure," Air Force Report AFCRL-TR-74-0560 (DTIC #AD-A008-490), August 30, 1974.
36. O. M. Aliev and R. A. Azadaliev, *Russ. J. Inorg. Chem.* **25**(11), 1732 (1980.
37. L. Ben-Dor and I. Shilo, *J. Solid State Chem.* **35,** 278 (1980).
38. M. Palazzi and S. Jaulmes, *Mater. Res. Bull.* **13** 1153 (1978).
39. V. Tien, J. Flahaut, and L. Domange, *C. R. Acad. Sci. Paris C* **262,** 278 (1966).
40. A. Tomas, M. Guittard, and J. Flahaut, *Acta Crystallogr. Sect. B* **42,** 364 (1986).
41. A. Tomas, V. Tien, M. Guittard, and J. Flahaut, *Mater. Res. Bull.* **20,** 1027 (1985).
42. F. H. A. Vollebregt and D. J. W. IJdo, *Acta Crystallogr. Sect. B* **38,** 2442 (1982).
43. O. Muller and R. Roy, "The Major Ternary Structural Families," pp. 77, 270, 272, 273, Springer-Verlag, New York, 1974.
44. J. Flahaut, L. Domage, M. Patrie, A-M. Bostsarron, and M. Guittard, *in* "Nonstoichiometric Compounds," Adv. in Chem. Series, Vol. 39, p. 179. American Chemical Soc., Washington, DC, 1963.
45. J. Flahaut, M. Guittard, M. Patrie, M. P. Pardo, S. M. Golabi, and L. Domange, *Acta Crystallogr.* **19,** 14 (1965).
46. J. Flahaut, L. Domange, and M. Patrie, *Bull. Soc. Chim. Fr.*, 2048 (1962).
47. M. O'Keeffe and S. Andersson, *Acta Crystallogr. Sect. A* **33,** 914 (1977).
48. J. E. Iglesias and H. Steinfink, *J. Solid State Chem.* **6,** 119 (1973).
49. H. Haeuseler, *J. Solid State Chem.* **86,** 275 (1990).
50. I. D. Brown and R. D. Shannon, *Acta Crystallogr. Sect. A* **29,** 266 (1973).
51. I. D. Brown, *in* "Structure and Bonding in Crystals," Vol. II, p. 1. Academic Press, New York, 1981.
52. N. E. Brese and M. O'Keeffe, *Acta Crystallogr. Sect. B* **47,** 192 (1991).
53. M. O'Keeffe, *Acta Crystallogr. Sect. A* **33,** 924 (1977).
54. A. Tomas, I. Shilo, and M. Guittard, *Mater. Res. Bull.* **13,** 857 (1978).
55. Powder Diffraction File, PDF #32-1242, 32-1254, 32-1272, 33-1327, 42-1493, 42-1494, 42-1495, 42-1496, 42-1497, 42-1498, 42-1499, 42-1500. JCPDS International Centre for Diffraction Data, Newtown Square, Pennsylvania, 1992.